2.3.3.1.2. *Crystallite-size effects*

In addition to profile broadening, which begins to appear when the crystallite sizes are < 1–$2\,\mu m$, the sizes have a strong effect on the absolute and relative intensities (de Wolff, Taylor & Parrish, 1959; Parrish & Huang, 1983). The particle sizes have to be less than about $5\,\mu m$ to achieve 1% reproducible relative intensities from a stationary specimen in conventional diffractometer geometry (Klug & Alexander, 1974). The statistical errors arising from the number of particles irradiated can be greatly reduced by using smaller particles and rotating the specimen around the diffraction vector. This brings many more particles into reflecting orientations.

The particle-size effect is illustrated in Fig. 2.3.3.2 for specimens of NIST silicon standard powder 640 sifted to different size fractions. The powders were packed in a 1 mm deep cavity in a 25.4 mm diameter Al holder using 5% collodion/amyl acetate binder. They were rotated by a synchronous motor (a stepper motor can also be used) around the axis normal to the centre of the specimen surface with the detector arm fixed at the peak position and the intensity recorded with a strip-chart. Rapid rotation, $\sim 60\,r\,min^{-1}$, gives the average peak intensity for all azimuths of the specimen and the small variations result only from the counting statistics. Scaling the intensities to (111) = 100% for the 5–10 μm fraction, the 10–20 μm fraction is 94%, 20–30 μm 88% and > 30 μm 59%. The decrease is probably due to lower particle-packing density and increasing interparticle microabsorption. The > 5 μm fraction = 95% may be due to the larger ratio of oxide coating around the particles to the mass of the particles.

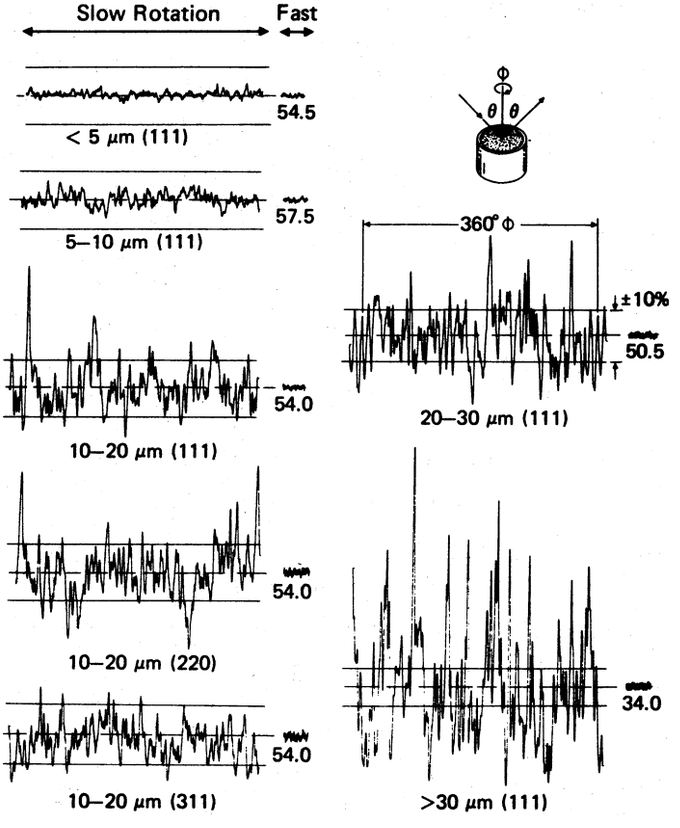

Fig. 2.3.3.2. Effect of specimen rotation and particle size on Si powder intensity using a conventional diffractometer (Fig. 2.3.1.3) and Cu $K\alpha$. Numbers below fast rotation are the average intensities.

Slow rotation, $\sim 1/7\,r\,min^{-1}$, shows the variation of the peak intensity with azimuth angle φ. The pattern repeats after 360° rotation and the magnitude of the fluctations increases with increasing particle sizes and resolution. There is no correlation between the fluctations of different reflections, as can be seen by comparing the 111, 220 and 311 reflections of the 10–20 μm specimen (lower left side) for which the incident-beam intensity was adjusted to give the same average amplitude. The horizontal lines are ±10% of the average. This shows the magnitude of errors that could occur using stationary specimens. Similar particle-size effects were found using the integrated intensities derived from profile fitting. The above discussion and Fig. 2.3.3.2 refer to a continuous scan. If the step-scan mode is used to collect data, it is clearly not necessary to rotate the specimen through more than one revolution at each step.

The rotating specimen also averages the in-plane preferred orientation but has virtually no effect on the planes oriented parallel to the specimen surface. The slow rotation method is useful in testing the grinding and sifting stages in specimen preparation. When calibrated with known size fractions, it can be used as a rough qualitative measure of the particle sizes.

2.3.3.2. *Problems arising from the Kα doublet*

A common source of error arises from the $K\alpha$ doublet which produces a pair of peaks for each reflection. The separation of the Cu $K\alpha_1$, $K\alpha_2$ peaks increases from 0.05° at 20°2θ to 1.08° at 150°2θ. The overlapping is also dependent on the instrument resolution and may cause errors in the peak angles and intensities when strip-chart recording or peak-search methods (described below) are used. The $K\alpha_1$ wavelength is generally used to calculate all the d's even when the low-angle peaks are unresolved. In the region where the doublet is only slightly resolved, the apparent $K\alpha_1$ peak angle is shifted to higher angles because of the overlapping $K\alpha_2$ tail and similarly the peak intensities will be in error. The relative peak intensities of a reflection with superposed doublet compared to a resolved doublet could have an error as large as 50%. Relative peak intensities are used in the ICDD standards file and cause no problem because the unknowns are measured in the same way. The integrated intensity avoids this difficulty but is impractical to use in routine identification.

Rachinger (1948) described a simple graphical procedure for removing $K\alpha_2$ peaks. The method causes errors because it makes the incorrect assumption that $K\alpha_2$ is the exact half-scale version of $K\alpha_1$. Ladell, Zagofsky & Pearlman (1975) developed an exact algorithm using the actual mathematical shapes observed with

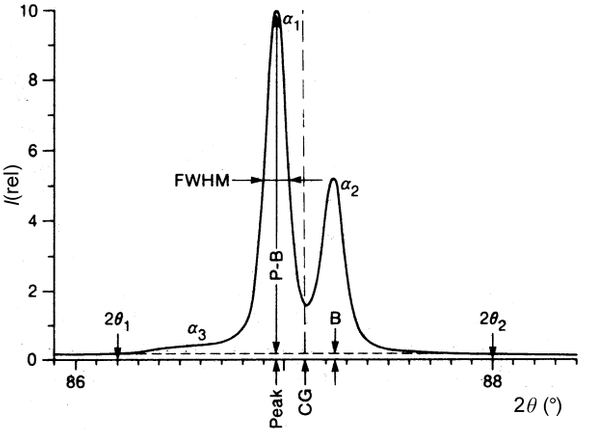

Fig. 2.3.3.3. Various measures of profile.

the user's diffractometer but, with line-profile-fitting programs now available, the $K\alpha_2$ component can be modelled precisely along with the $K\alpha_1$.

It is possible to isolate the $K\alpha_1$ line when using a high-quality incident-beam focusing monochromator as described in Subsection 2.3.1.2, Fig. 2.3.1.12(*b*), but there may be a loss of intensity. The source size must be narrow and the focal length long enough to separate the components.

2.3.3.3. *Use of peak or centroid for angle definition*

The most obvious and commonly used measure of the reflection angle of a profile is the position of maximum intensities (Fig. 2.3.3.3). The midpoints of chords at various heights have often been used but their values vary with the profile asymmetry. Another method is to connect the midpoints of chords near the top of the profile and extrapolate to the peak. The computer methods using derivatives are the most accurate and fastest as described in Subsection 2.3.3.7.

A more fundamental measure that uses the entire intensity distribution is the centre of gravity (or centroid) defined as

$$\langle 2\theta\rangle = \int 2\theta I(2\theta)\,\mathrm{d}(2\theta) \Big/ \int I(2\theta)\,\mathrm{d}(2\theta). \qquad (2.3.3.5)$$

The variance (mean-square deviation of the mean) is defined as

$$W_{2\theta} = \langle(2\theta - \langle 2\theta\rangle)^2\rangle = \int(2\theta - \langle 2\theta\rangle)^2 I(2\theta)\,\mathrm{d}(2\theta) \Big/ \int I(2\theta)\,\mathrm{d}(2\theta). \qquad (2.3.3.6)$$

The use of the centroid and variance has two important advantages: (1) most of the aberrations (§2.3.1.1.6) were derived in terms of the centroid and variance; and (2) they are additive, making it easy to determine the composite effect of a number of aberrations. Mathematically, the integration extends from $-\infty$ to $+\infty$ but the aberrations have a finite range. However, the practical use of these measures causes some difficulty. If the profile shapes are Lorentzian, the tails decay slowly. A very wide range would be required to reach points where the signal could no longer be separated from the background and the profiles must be truncated for the calculation. Truncation limits that have been used are 90% ordinate heights of $K\alpha_1$ (Ladell, Parrish & Taylor, 1959), and equal 2θ or λ limits from the centroid (Taylor, Mack & Parrish, 1964; Langford, 1982). The limits such as $2\theta_1$ and $2\theta_2$ in Fig. 2.3.3.3 must be carefully chosen to avoid errors and this involves the correct determination of the background level. It is not practical to use centroids for overlapping peak clusters unless the profile fitting can accurately resolve the individuals with their correct positions and intensities. Their use has, therefore, been confined to simple patterns with small unit cells in which the profiles were well separated.

The difference between the angle derived from the peak and the centroid depends on the asymmetry of the profile, which in turn varies with the $K\alpha$-doublet separation and the aberration broadening. Tournarie (1958) found that the centre of a horizontal chord at 60.6% of the $K\alpha_1$ peak height corresponds well to the centroid of that line in fairly well resolved doublets. The number, of course, depends on the profile shape. There is also the basic problem that most of the X-ray wavelengths were probably determined from the spectral peaks and, if the centroids are measured for the powder pattern, the Bragg equation becomes nonlinear in the sense that the 1:1 correspondence between λ and $\sin\theta$ is lost.

2.3.3.4. *Rate-meter/strip-chart recording*

Formerly, the most common method of obtaining diffractometer data was by using a rate-meter and strip-chart recorder with the paper moving synchronously with the constant angular velocity of the scan. This simple analogue method is still used and a large fraction of the JCPDS (ICDD) file prior to about 1982 was obtained in this way.

The method has several limitations: the data are not in the digital form required for computers, and are distorted; manual measurement of the chart takes a long time and has low accuracy. The output of the strip chart lags behind the input by an amount determined by the product of the scanning speed and the time constant of the rate-meter, including the speed of the recorder pen. The peak height is decreased and shifted in the direction of the scan causing asymmetric broadening with loss of resolution. The profile shape, $K\alpha$-doublet separation, and scan direction also contribute to distortion. When the product of the scan speed and time constant have the same value, the profile shapes are the same even though the total count is determined by the scan speed, Figs. 2.3.3.4(*a*) and (*b*). If the product is large, the distortion is severe (*c*), and very weak peaks may be lost.

2.3.3.5. *Computer-controlled automation*

Most diffractomers are now sold with computer automation. Older instruments can be easily upgraded by adding a stepping motor to the gear-drive shaft. A large variety of computers and programs is available, and it is not easy to make the best selection. Continuing improvements in computer technology have been made to handle expanded programs with increased speed and storage capabilities. The collected data are displayed on a VDU screen and/or computer printer and stored on hard disk or diskette for later use and analysis. Microprocessors are often used to select the X-ray-generator operating conditions, shutter control, specimen change, and similar tasks that were formerly performed manually. Aside from the elimination of much of the manual labour, automation provides far better control of the data-collection and data-reduction procedures. However, computers do not preclude the necessity of precise alignment and calibration. Smith (1989) has written a detailed description of computer analysis for phase identification and also includes related programs and their sources.

Personal computers are widely used for powder-diffraction automation and a typical arrangement is shown in Fig. 2.3.3.5(*a*). The automation may provide for step scanning,

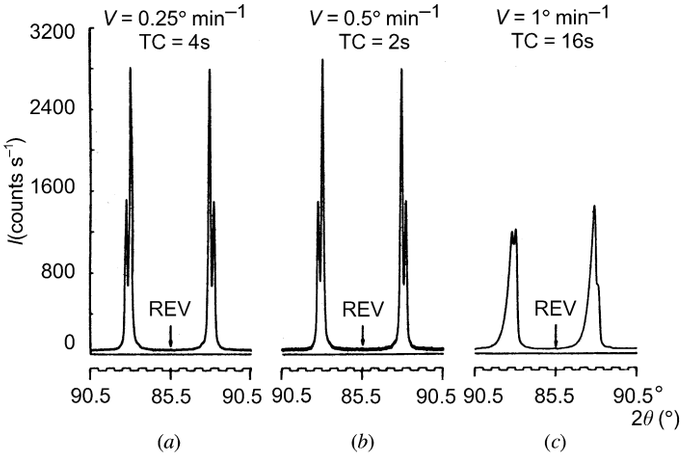

Fig. 2.3.3.4. Rate-meter strip-chart recordings. REV: scan direction reversed. Scan speed and time constant shown at top.

references